Intracellular DNA Cargo Release from a Gold Nanoparticle Modulated by the Nature of the Surface Coupling Functionality

Kate J. F. Carnevale[iD] and Geoffrey F. Strouse*[iD]

Department of Chemistry and Biochemistry, Florida State University, Tallahassee, Florida 32306-4390, United States

S *Supporting Information*

ABSTRACT: Covalently coupling nucleic acids to a gold nanoparticle (AuNP) surface has been demonstrated for generating effective gene therapy agents to modify cellular protein expression. The therapeutic efficacy of the approach is anticipated to be impacted by the length of time the nucleic acid sequence resides in the endolysosomal pathway once transfected into a cell. It is believed that the dynamics of the processing should reflect the linkage chemistry of the DNA to the AuNP surface. In this manuscript the dynamics of nanotherapeutic uptake, nucleic acid release, and gene processing are investigated *in vitro* for a AuNP-nucleic acid delivery platform transfected into A375 human melanoma cells, as a function of the nucleic acid-gold linkage chemistry.

The dynamics of cell processing of the single monodentate thiol (SX), bidentate dual thiol (SS), or mixed bidentate thiol plus amine (SN) coordination of nucleic acids to the AuNP surface are evaluated using a multicolor nanosurface energy transfer bio-optical transponder (SET-BOT) technology. The use of live-cell fluorescence microscopy allows for the direct visualization of the uptake and localization of a lipofectamine-packaged SET-BOT using a dye (DL700) that is not quenched in the proximity of the AuNP, while fluorescence "turn on" of a dye that is proximally quenched by the AuNP (DL488) is used to report on the dynamics of release of the nucleic acid cargo within the cell. For protein expression following transcription of the gene, the emission signature of a red fluorescent protein, tdTomato, is monitored. The intracellular rates of DNA release from the AuNP surface once endosomally packaged within the A375 human melanoma cells were found to follow the binding activity series: bidentate thiol > bidentate thiol plus amine > monodentate thiol, consistent with the strength of multidentate chelation, paired with the stabilizing influence of π-backbonding of thiols compared to σ-donation in amines, when bound to a gold surface.
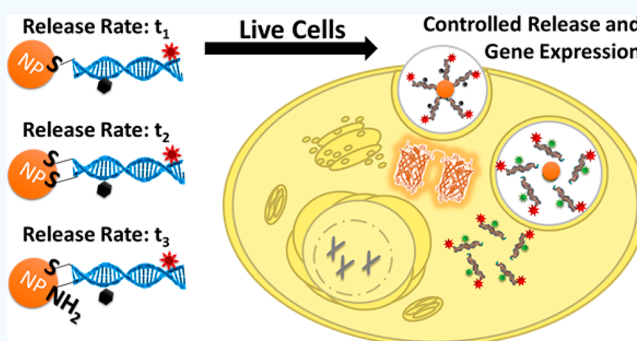
INTRODUCTION

The ability to image events live *in vitro* has skyrocketed in the last few decades due to technological advancements in instrumentation and new methodologies for cellular and molecular visualization.[1] Recent innovations in this field reflect the use of live-cell fluorescence microscopy and Surface Energy Transfer (SET) based nanoparticle bio-optical transponders (BOT).[2−6] In parallel with development of biophysical tools utilizing nanoprobes for cellular interrogation, the ability of nanomaterials to load multiple therapeutic agents has been established for a variety of nanoparticle-bioconjugate constructs.[7−10] The pairing of such techniques has been shown to be effective in spatiotemporal mapping of intracellular phenomena in real time, including delivery of therapeutic agents and endosomal pH levels.[11−13] Attempts to intentionally modulate cellular metabolites has led to *in vitro* studies using the AuNP as a delivery agent of full plasmids and siRNA for knocking-in and knocking-out fluorescent protein expression.[7,12−14] Although protein expression modulation is observed, the mechanism and endolysosomal metabolites that are involved in controlling the timing of release of the plasmids from the AuNP surface is not well understood.

Several researchers have demonstrated the ability to control release through the use of external signals, such as chemical activation or using electromagnetic radiation to heat and melt the particle to induce therapeutic cargo release.[15−17] However, while exciting for *in vitro* studies, these approaches are difficult to control for agents attached to the same nanoparticle delivery vehicle, and likely would complicate a realistic treatment approach in a living patient, where systemic interactions are possible and direct observation of the cells being treated is not. A more pragmatic approach to controlled therapeutic release lies in utilizing surface appendage chemistry to control the dynamics of nanoparticle release in cellular environments. It is postulated that cellular reducing agents and changes in pH levels likely play a role, suggesting the nature of coordination may allow the timing of release to be manipulated.[12,18,19] The role of σ- and π-bonding interactions on stabilizing the metal to ligand bond for typical functional groups (RCOOH, -NH$_2$, -SR, -PR$_3$, etc.) is well studied for gold.[20−25] Researchers have

shown that thiols bind strongly to gold surfaces due to π-backbonding between the metal d-orbitals and empty p-orbitals on the sulfur.[26,27] Similar arguments have been made to understand binding of amines, carboxylates, imidazoles, or ether functionalities at a gold surface.[7,19,25,28−32] Analogous to findings in inorganic coordination chemistry, enhanced stability of the surface appended biomolecules has also been reported for ligands with the potential for multichelation, as exemplified by hexa-histidine ligand binding,[28,32] the use of dihydrolipoic acid links to stabilize coordination of polymer chains,[25,33−36] or chelation of duplex DNA to a AuNP surface through two thiol linkages via the 5′ and complementary strand 3′ phosphate backbone modification.[6,31]

In the current work, the control of intracellular release of nucleic acids cargoes covalently coupled through mono- and bidentate thiol and amine functional groups at the surface of a 6 nm AuNP is investigated by employing a multicolor surface energy transfer (SET) bio-optical transponder (BOT) to monitor uptake and release of a Dylight 488 (DL488) and Dylight700 (DL700) labeled short, 39 base pair (bp) DNA, as well as a dye labeled 6 kbp plasmid gene designed to initiate production of the red fluorescent protein (RFP), tdTomato, following transcription. The nucleic acid cargoes are bound to the surface of the gold by appending a functionalized C_6 spacer from phosphate backbone (DNA-PO_3O-C_6H_{12}-X, where X is -NH_2 or -SH). Functionalization of the 3′ end of one single strand and the 5′ end of the complementary single strand of a DNA duplex allows the intracellular endolysosomal stability of a monodentate thiol (DNA modified at the 3′ only), a bidentate dual thiol (3′ and comp 5′ DNA modifications), and a mixed bidentate thiol plus amine coupling (3′ and comp 5′ DNA modifications) bound to a AuNP to be explored. It is hypothesized that the strength of covalent attachment of the therapeutic cargo to the AuNP will follow bidentate thiol (SS) > bidentate thiol plus amine (SN) > monodentate thiol (SX). The SET-BOT probe design allows monitoring of the intracellular processing of the SET-BOT through tracking of DL700, which does not exhibit energy coupling to the AuNP, and by measuring the kinetics of intracellular release of nucleic acids form the AuNP surface through the "turn-on" of the DL488 fluorescent marker. Analysis of the turn-on events and colocalization of the DL700 and DL488 provide the kinetics of intracellular uptake and processing to be analyzed for each coupling strategy in real time, via live cell fluorescence microscopy. Understanding and utilizing AuNP surface chemistry that is able to produce controllable, self-terminating conjugation of biologically active cargo to the nanodelivery agent may allow for the design of tunable release of therapeutics once transfected into the intracellular environment. Advances in this technology have the potential to control metabolite knock-in versus knockout timing in biomedical studies. With the advancements in delivery and imaging, it can be imagined that control over the timing and location of delivered drugs or genes inside of target cells, such as cancers or diseased tissue, could lead to insights relevant to biomedical applications, such as controlled drug delivery and coordinated gene therapy approaches for improved treatment and prevention of disease.

■ RESULTS AND DISCUSSION

SET-BOT Construct Design. In Figure 1, the design of the SET-BOT to test the influence of coupling strategies to manipulate the timing of nucleic acid release from a 6 nm
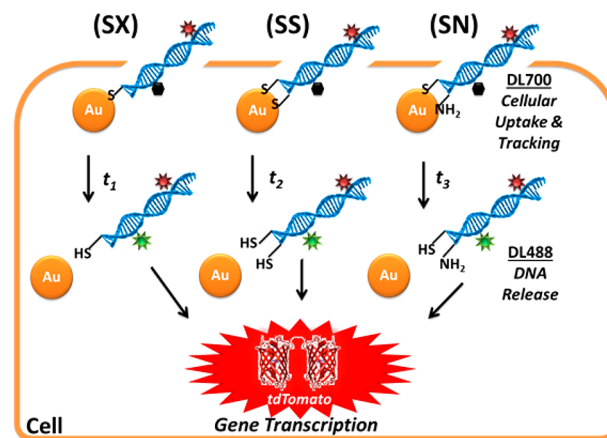
Figure 1. Scheme of AuNP-DNA coupling strategy, showing monodentate thiol (SX), bidentate dual thiols (SS), and mixed bidentate thiol plus amine (SN) coordination of the DNA to the AuNP with corresponding anticipated release times: t_1, t_2, and t_3, respectively. Cellular uptake is monitored by constant DyLight (DL) 700 emission, release from the AuNP is monitored by turn on of DL488, according to SET theory, and gene expression is observed by emission of the red fluorescent protein dimer, tdTomato.

diameter AuNP once endocytosed is shown schematically for the appendage of a 39-mer duplex DNA sequence to the AuNP surface. The 6 nm AuNP is prepared by literature methods utilizing citrate as a reducing agent[37] and the surface bound citrate ligands are exchanged for bis(sulfonatophenyl)phenyl phosphine (bSPP)[2] prior to coordination of the functionalized nucleic acid sequences. Use of the negatively charged bSPP ligand as a AuNP surface passivant reduces electrostatic interactions that can lead to nonspecific DNA backbone coupling at the AuNP surface. Size distributions of the as-synthesized AuNPs are extracted from transmission electron microscopy (TEM) images, and the data is available in the Supporting Information (Supporting Information Figure SF1A).

The duplex DNA studies are carried out on a 39-mer containing a 4 base overhang (35 base pair-duplex, and 4 bases of single stranded DNA). The overhang is intentional to allow ligation of the linearized 6 kbp plasmid for the plasmid expression study. The 39 mer DNA incorporates two C_6 functionalized linkers (3′ and 5′ end modification) for coupling to the AuNP surface and two reporter fluorophores incorporated via a modified thymine (T). The dyes are incorporated to unique strands of the duplex (DNA sequences provided in Supporting Information). The single stranded 35 mer incorporates a variable functionality at the 5′ end using a C_6-linker containing no modification(X), an amine (−NH_2) or a thiol (-SH) for coupling to the AuNP surface, as well as a DL488 "release sensor" label at the seventh position relative to the AuNP surface. The complementary 39-mer has a 3′-C_6-thiol (SH) modification to the single stranded DNA sequence and incorporates theDL700 "uptake sensor" appended at the 30th bp relative to the AuNP surface (11th base pair from 5′ end). The duplex was annealed prior to coupling to the AuNP surface by slow-cool annealing procedures to produce duplexed nucleic acid sequences with 3′ monodentate thiol (SX), 3′ and 5′ bidentate dual thiols (SS), and bidentate 3′ thiol with 5′ amine (SN) binding moieties.

For the 6 kbp linearized plasmid studies, the plasmid was attached to the 39-mer sequence, mentioned above, to provide

the surface linkers (SX, SN, and SS) and the fluorophore labels (DL700 and DL488). The linearized gene sequence is cut from a circular plasmid containing the gene for the red fluorescent protein (RFP), tdTomato, and a cytomegalovirus (CMV) promotor to drive overexpression[38] of the tandem dimer RFP. The plasmid was assembled onto the AuNP utilizing ligation of the linearized plasmid sequence to the labeled 39-mer DNA duplex sequence. Prior to ligation, the plasmid was linearized using the restriction enzyme, PciI (New England Biolabs), which leaves a 4 base overhang. The linearized plasmid was isolated using ethanol precipitation. The 39-mer DNA duplex contains the complementary 4 base overhang to allow for direct ligation of the linearized plasmid to the dye labeled 39-mer duplex using DNA T4 ligase (New England Biolabs), by methods previously reported.[2] Evidence of the successful linearization can be seen in the agarose gel of the circular *versus* restricted linearized plasmid (Supporting Information Figure SF2A), and successful coupling to the AuNP surface is shown *via* the agarose gel of the AuNPs with appended genes *versus* as-synthesized AuNPs (Supporting Information Figure SF2B). For ease of reference, the tdTomato plasmid gene will be abbreviated as TSX-, TSS-, and TSN-Gene, respectively, to identify the linkage chemistries and DNA length. The plasmid SET-BOT probe allows for the reporting of uptake, timing of release, and correlation with gene expression of the tdTomato fluorescent protein as a mimic for gene therapy applications.

Appending Nucleic Acid to AuNP. In order to append the DNA to the AuNP, reduction of the synthetic dithiol protecting groups was accomplished through incubation with 5 mM tris(2-carboxyethyl)phosphine (TCEP), to deprotect the dithiolated DNA, after which the synthetic DNA was added directly to the AuNP at a 20:1 DNA to AuNP ratio, with a 24–48 h mixing period to allow for DNA attachment. Although not explicitly shown in Figure 1, the 6 kbp linearized plasmid bound to the AuNP surface is assembled onto the AuNP surface in analogy to the 39-mer short DNA.

Characterization of the SET-BOT. The UV−visible absorption profile of the as-synthesized AuNP compared to the DNA-complexes shows the appearance of the 260 nm DNA peak, a shoulder arising from the DL488 absorption near 490 nm, and the DL700 peak at 700 nm, in addition to the 525 nm AuNP plasmon, when the DNA strands are appended (Figure 2A). Calculation of the DNA loading levels on the AuNP was performed by comparing the absorbance of the 260 nm DNA peak, corrected for AuNP absorption, compared to the 525 nm plasmon of the AuNP. The loading ratios were found to be 20:1 DNA:AuNP for AuNP-SX-DNA, 12:1 for AuNP-SS-DNA, and 16:1 for AuNP-SN-DNA. Similar loading levels are observed for the AuNP-plasmid studies. Observed differences in loading between the experimental attachment strategies may be due to steric repulsion forces for the bidentate coordination approach or due to the higher likelihood of a bidentate coordination displacing the BSPP ligands. Additionally, the successful coupling of the DNA to the AuNP was evaluated by 1% agarose gel electrophoresis, which demonstrated retention of the AuNP-DNA complexes compared to the AuNP-bSPP due to the increased molecular weight of the attached DNA (Figure 2B).

For reference, the idealistic maximum possible number of DNA molecules able to bind to the 6 nm AuNP surface was calculated based on molecular diameter alone (ignoring more complex steric and molecular interactions), where the area of a 6 nm AuNP is ∼113 nm^2, and the footprint of a
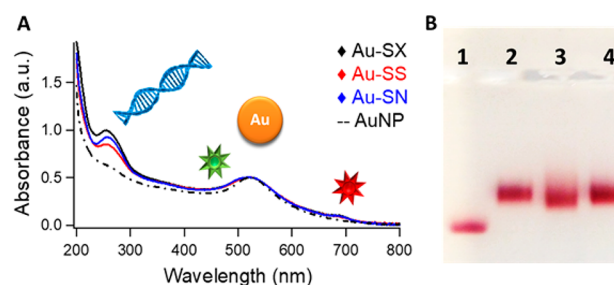

Figure 2. Characterization of the AuNP-DNA constructs showing (A) UV−visible absorption spectroscopy of the as-synthesized AuNP-bSPP (black dashed line), with the monodentate thiol appended DNA (black solid line), the bidentate thiol appended DNA (red solid line), and the mixed bidentate thiol plus amine appended DNA (blue solid line). DL700 peak at 700 nm, AuNP peak at 525 nm, DL488 shoulder at 490 nm, and DNA peak at 260 nm. (B) 1% agarose gel electrophoresis of the AuNP-bSPP (1), AuNP-SX-DNA (2), AuNP-SS-DNA (3), and AuNP-SN-DNA (4) showing red bands indicative of the plasmonic absorption of the AuNPs.

perpendicularly attached 2 nm diameter DNA molecule is 3.14 nm^2. Thus, the maximal loading level of DNA for this 6 nm AuNP would be 36 DNA per AuNP. However, prior to DNA addition, the AuNPs are passivated with bSPP (diameter of ∼1 nm) to increase particle stability and prevent DNA molecules from laying their phosphate backbone down on the AuNP surface. This means that, as observed experimentally, the actual DNA loading levels are reduced from the calculated ideal value due to the need to displace bSPP molecules prior to DNA binding. Although only one size of AuNP was explored for this work, it can be assumed that by increasing the AuNP size, and thereby increasing the particle's surface area, more DNA would be able to bind to the AuNP to create a larger deliverable payload. However, with increasing AuNP size also comes a reduction in the particle's surface curvature, which would increase steric repulsion forces of the DNA molecules as their highly charged phosphate backbones are forced into tighter packing arrangements.[33,39,40] Thus, optimization of particle size and loading level may be useful depending on the nature of future clinical applications.

Evidence of SET-BOT assembly is also provided by dynamic light scattering (DLS). The DLS data in Figure 3 shows a change in hydrodynamic radii for AuNP-bSPP *versus* AuNP-DNA and AuNP-plasmids. Additionally, Figure 3 shows the hydrodynamic sizes as assessed for each SET-BOT within the commercial transfection reagent Lipofectamine2000, to determine the change in size due to encapsulation within a cationic liposome. The DLS data shows an increase in hydrodynamic diameter from AuNP-bSPP (∼14 nm) < AuNP-DNA (∼46 nm) < AuNP-plasmid (∼132 nm), as is expected for successfully assembled constructs. It is postulated the change in size for the AuNP-DNA systems reflects tilting at the AuNP surface for the monothiol *versus* bidentate systems, as well as DNA loading differences. For the AuNP-plasmid, the coiling of the 6 kbp gene dominates the hydrodynamic ratio and no statistical difference in size is observed. Additional comparison of hydrodynamic size for the liposome encapsulated transfection packages found only a slight increase in size was observed for the lipid encapsulated gene constructs, but a larger size increase was apparent for the short DNA and non-DNA functionalized AuNPs, likely due to differences in charge density from the decreased anionic contribution from DNA phosphate backbone with decreased (or absent) DNA length
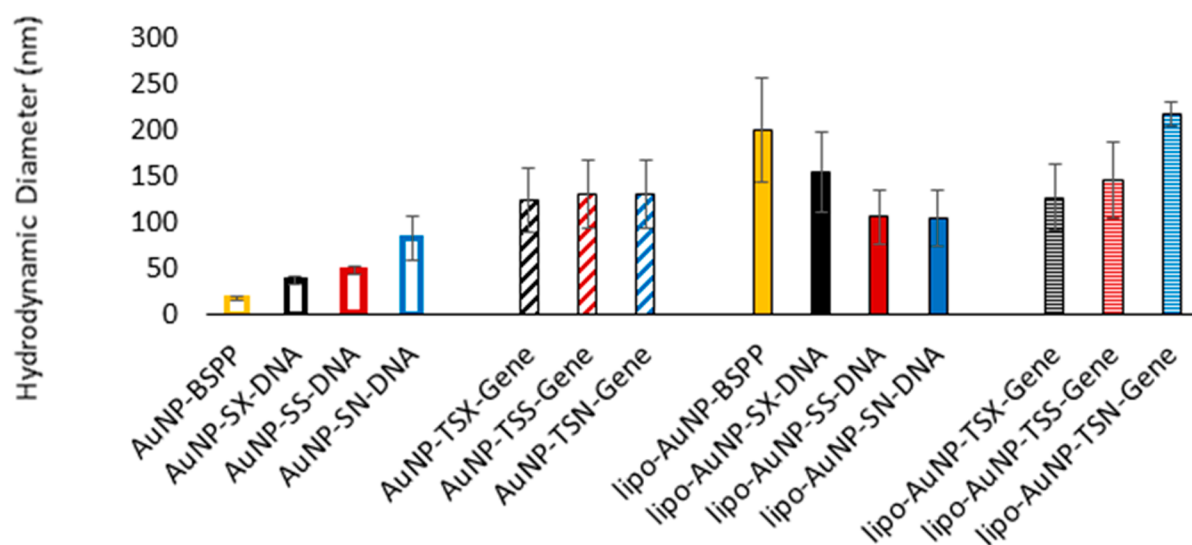
Figure 3. Dynamic light scatter of as-synthesized AuNP-bSPP, with short DNA and plasmid Gene appended by monodentate thiol (SX/TSX), bidentate thiol (SS/TSS), mixed bidentate thiol plus amine (SN/TSN), alone and encapsulated within Lipofectamine2000 (lipo) transfection reagent. Error bars represent deviation.

(Figure 3). The variations in hydrodynamic sizes observed for the different chemical appendage strategies of AuNP-DNA and AuNP-plasmid constructions are within experimental error for the measurements.

The design of the system allows verification of the SET-BOT assembly by analysis of the change in the individual fluorophore intensity for the fluorophore labels on the nucleic acid sequence when bound to and when released from the AuNP surface following the AuNP dissolution reaction with cyanide ions (Supporting Information SF3).[12,41] Complete etching of the AuNP is carried out on the same sample exposing the assembled complexes to a 0.1 M NaCN solution, which can be verified by the loss of the AuNP absorption plasmon at 525 nm (Supporting Information Figure SF3A). SET theory predicts that the DL700 appended to the 30th bp from the AuNP surface will not be SET active, while the appended DL488 at the seventh bp position will be SET active.[42,43] At the distance of AuNP surface for DL488, the DL488 emission intensity is theoretically reduced by >90% due to efficient energy coupling to the surface plasmon on the AuNP, as described by SET theory.[42,43] In addition, the DL488 to DL700 energy transfer via Förster mechanism is <1% at the separation distance on the sequence. In Supporting Figure SF3, the emission profiles for the DL488 (λ_{ex} = 488 nm, 298 K) and DL700 (λ_{ex} = 700 nm, 298 K) in DI H$_2$O in cuvette are shown before and after cyanide etching of the attached AuNP. Evaluation of the emission data shows the DL488 exhibits recovery of the emission intensity when compared to free DL488 at identical conditions, while the DL700 signal was unaffected (Supporting Information Figure SF3B,C). The SET validation experiment confirms the assembly of the SET-BOTs, consistent with the agarose gel and DLS observations. As an added note, cyanide treatment can affect the PL properties of FAM, but for DyLight dyes there was no observed adverse effect on the photophysical properties of the dyes used within the experimental time scale (15−30 min of coincubation), although at long treatment times (>4 h of coincubation) the DL488 and especially DL700 were observed be degraded in the presence of the cyanide salt, as indicated by a loss of absorption and emission features (data not shown).

Cell Transfection and Imaging. The uptake and processing of the SET-BOTs (SX/SS/SN-DNA and TSX/TSS/TSN-Gene) were analyzed in human melanoma cells, A375, plated in 96-well plates with glass bottoms and were incubated at 37 °C using a live cell chamber mounted on the microscope stage. The cells were transfected 24 h after plating using Lipofectamine2000 transfecting reagent containing 2.6 μM AuNP-SX/SS/SN-DNA and AuNP-TSX/TSS/TSN-plasmid complexes. Cell viability was analyzed using trypan blue staining to confirm >90% cell viability in all experiments (data not shown).

The optical images showing the individual color channels and an overlay are presented in Figure 4 with larger images available in Supporting Information Figure SF4 for the specific linkage strategies for duplex DNA (Figure 4A-C) and for the linearized plasmid gene (Figure 4D-F). To better visualize the intracellular maturation of the SET-BOT packages via the fluorescence profiles from punctate (endosomally encapsulated) to diffuse (cytosolically escaped), digitally magnified individual cell images are available in the Supporting Information for the AuNP-SX/SS/SN-DNA constructs at 4 and 16 h post transfection (Supporting Information Figure SF5).

In Figure 4, differential interference contrast (DIC) brightfield images and fluorescence channel images of the transfected A375 cells are shown for selected time points from 0 h (initial transfection) to 48 h. Control experiments for a dithiol-protected nucleic acid, which remains unbound in the presence of the AuNP were performed (Supporting Information Figure SF6). The observed time dependent changes in emission intensity, cellular localization, and degree of colocalization of the fluorophores can be interpreted with respect to the fluorophore-AuNP SET response. The DL700, which is SET inactive, is always "on" providing dynamic monitoring of the nucleic acid location in the cell, while an emission "turn-on" signal for the SET active DL488 signals the moment of nucleic acid release from the AuNP surface. In all experiments, at early time points, DL488 and DL700 fluorescent packages are seen with punctate patterning inside of the cells, indicating endosomal packaging, as is expected
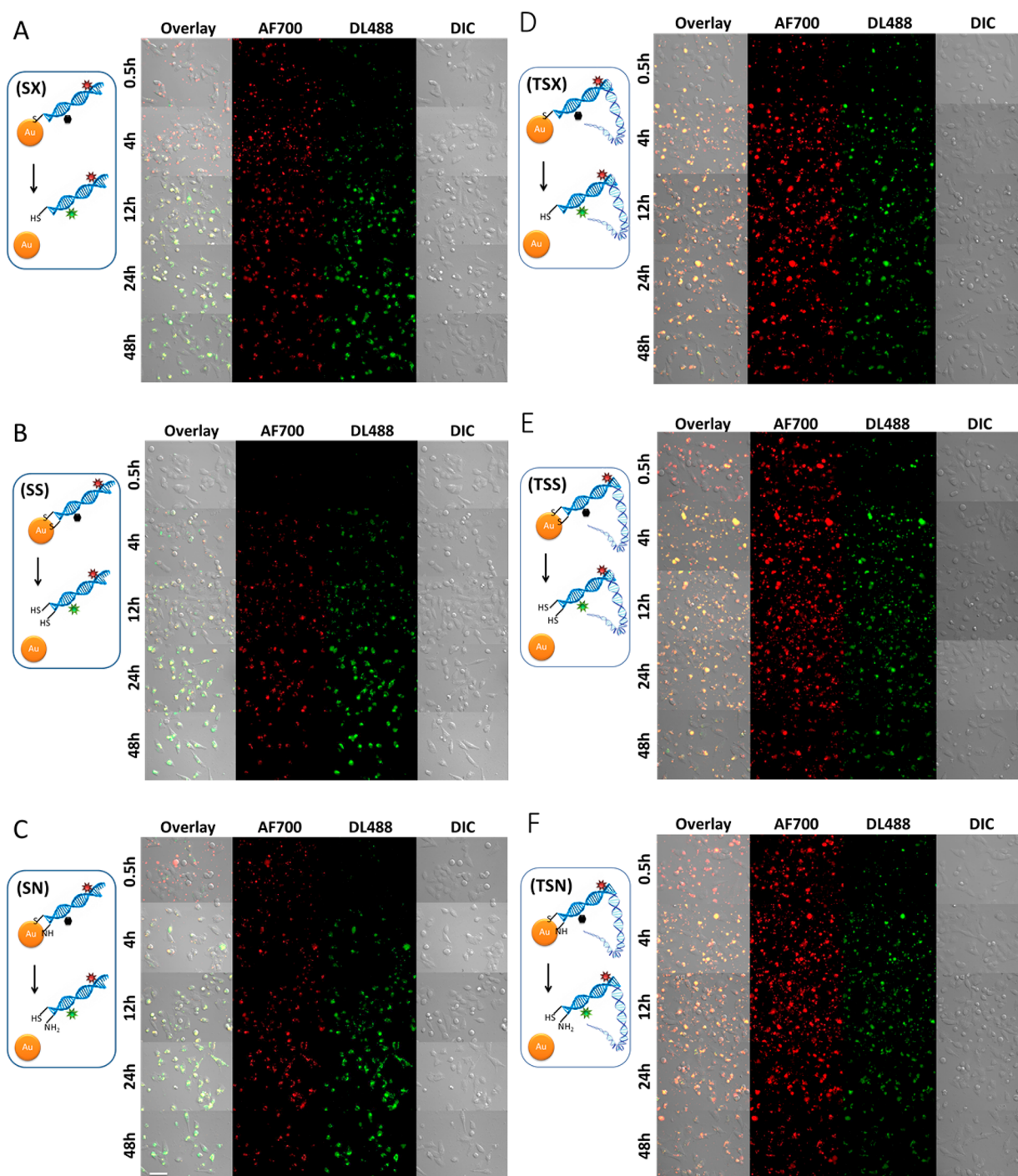
Figure 4. Live cell fluorescence microscopy images of A375 melanoma cells incubated with short DNA (A) AuNP-SX-DNA, (B) AuNP-SS-DNA, and (C) AuNP-SN-DNA and full plasmid gene (D) AuNP-TSX-Gene, (E) AuNP-TSS-Gene, and (F) AuNP-TSN-Gene over 48 h. DL700 denotes nanocargo tracking throughout the experiment, DL488 shows DNA-cargo release, brightfield DIC shows normal cell morphology, and overlay shows localization. Scale bar is 50 μm.

with the use of the cationic liposome (Lipofectamine2000) transfection reagent. It can be qualitatively observed that in the enlarged images of Figure 4 (Supporting Figure SF4) that for the DNA (SX/SS/SN) and plasmid gene (TSX/TSS/TSN) SET-BOTs during the transfection experiment the DL700 fluorescence signal is nearly constant, while the DL488 fluorescence is "off" at early time points and is observed to increase in intensity over time. Qualitatively the release rate appears to follow the predicted trend of (T)SS < (T)SN <

(T)SX. Closer inspection of the images reveals that the DL488 and DL700 appear within the same punctate packages early in the experiment consistent with endosomal packaging. At later time points, the cell images display diffuse fluorescence intensity throughout, indicating endosomal escape of the dye-labeled DNA and diffusion into the cytosol. Inspection of Supporting Figure SF5 illustrates that at the earlier time point, the majority of the SET-BOT packages are endosomally entrapped, depicted by punctate fluorescence, but by the 16 h

time point each SET-BOT construction has experienced some degree of cytosolic escape, as observed by the more diffuse cellular fluorescence patterning.

The coupling chemistry of DNA attachment to the AuNPs does not appear to qualitatively affect the uptake of the SET-BOT in time based upon the DL700 intensity in the fluorescence images (Figure 4). Plots of the average intensity of DL700 fluorescence in time, specifically assessed within the cellular boundaries, are provided in the Supporting Information (Supporting Figure SF7) to better analyze the cellular processing. From the plot, it can be seen that the short DNA complexes (Supporting Information Figure SF7A) appear to enter the A375 skin cancer cells at a steadier rate as compared to the larger plasmid containing AuNP vectors (Supporting Information Figure SF7B), which reach plateau values within ∼8 h, whereas the short DNA loaded AuNPs still show some degree of intensity increase up to 24 h, despite the majority of particles localizing within the cellular boundaries by 8 h. It is worth noting that variations in uptake profiles between the different assembly strategies may reflect differences in overall DNA loading onto the AuNP surface and related charge density effects within the cationic liposomes during formation, creating slightly differentially sized liposomes, which may experience nonuniform rates of cellular internalization due slower diffusion of larger liposome toward the cellular surface. As shown in Figure 3, the encapsulation of the SET-BOT in Lipofectamine2000 increases the hydrodynamic radii for all complexes, irrespective of coupling chemistry approach, and with only partial effect from DNA length (Figure 3). Variances in the sizes of the final packages likely reflects differences in the initial AuNP-DNA size, and any potential mixing rates SET-BOT and lipid molecules.

To ensure the changes in emission intensity for the fluorophores were due to cellular processing of the SET-BOT, the stability of the complexes was assessed in cuvette using serum containing cell culture media with AuNP complexes incubated at 37 °C for 48 h. It was found that over the experimental time frame, the majority of DNA did not release outside of the cellular environment, with greater than 70% of DNA remaining bound after 48 h for each AuNP-construction. Specifically, the monodentate thiol (AuNP-SX-DNA) showed release of 25%, the bidentate thiol (AuNP-SS-DNA) showed release of 21%, and the mixed bidentate thiol plus amine (AuNP-SN-DNA) showed release of 28% of the DNA bound to the AuNP surfaces, as compared to full release achieved though cyanide dissolution of the particles. (Supporting Information Figure SF8). These results indicate that the DNA release events from the AuNP surface are primarily activated by intracellular processes, such as exposure to cellular reducing agents and proteins, and not merely disassembly of the complexes due to salinity or the presence of serum proteins found in biological media. Although the exact mechanism of AuNP-DNA release is not known, the findings coincide with previous work on monodentate thiol attached DNA-AuNP systems.[12,44] Conversely, the surface chemistries of other diagnostically relevant nanomaterials, such as luminescent semiconductor quantum dots (QDs), have been shown to maintain attachment within cellular environments,[45] making the use of cleavable spacers located away from the particle surface a viable alternative for non-AuNP nanomaterials.[46]

Colocalization Analysis. Analysis of the degree of intracellular colocalization for the DL488 and DL700

fluorescent labels, each located on opposite complimentary DNA strands, was carried out on the microscopy images in order to evaluate any potential degradation of the nucleic acid sequences over the course of the experiment. The cross correlation function (CCF)[47] analysis of the DL488 and DL700 fluorescence channels for each SET-BOT construct is shown in Supporting Information Figure SF9 at 8, 12, and 24 h after transfection, for the short DNA and plasmid genes attached to the AuNP by the various coupling strategies. Assessment of the CCF method described by van Steensel and co-workers provides the most unbiased measure of colocalization for fluorophores with punctate fluorescence patterns, especially when the fluorophores possess differential fluorescence quantum efficiencies and detector sensitivities for their emission windows.[12] In CCF, the Pearson's correlation coefficient of colocalization (r_P, eq 1) is calculated for and compared between two potentially colocalizing fluorescence channels, "A" (DL700), versus "B" (DL488), as they are laterally shifted by 20 pixel increments.

$$r_p = \frac{\sum (A_i - a) x (B_i - b)}{\sqrt{\sum (A_i - a)^2 x \sum (B_i - b)^2}} \tag{1}$$

Here i denotes intensity values for a given pixel, and a and b denote the intensity averages over the whole image per channel, A and B.[48] The best Gaussian fit of the plot created by this lateral pixel shifting of the fluorescence images versus the calculated effect on the Pearson's correlation coefficient gives the CCF.[47,49] Inferences about the colocalization are drawn from the overall shape and amplitude of the CCF plot, where maxima at the 0 pixel shift position indicates the presence of colocalization, and the amplitude (0−1) indicates the degree of spectral intensity matching between the channels.[47,49]

The CCF analysis of the data in Figure 4 shows Gaussian shaped distributions are observed indicative of colocalization of DL700 and DL488 at the 8, 12, and 24 h time points (Supporting Information Figure SF9). The observed correlation behavior supports an assumption that over the course of the study no significant endosomal degradation of the nucleic acid occurred, allowing the intensity behavior in Figure 4 to be used to qualitatively evaluate release behavior for the nucleic acid sequence as a function of the coupling strategy.

Dynamics of In Vitro Nucleic Acid Release. In Figure 5, the analysis of the time-dependent fluorophore emission intensity is plotted to extract the kinetics for the release of the nucleic acid from the AuNP surface using the appearance of the DL488 emission. A plot of the normalized intensity versus time for DL488 is shown in Figure 5. Analysis of the intensity per cell provides a quantitative measure of the dynamics for intracellular release for the AuNP-SX/SS/SN-DNA and AuNP-TSX/TSS/TSN-Genecoupling strategies. The kinetics are extracted by analyzing the DL488 intensity by processing the microscopy images using FIJI[50] ImageJ software to collect total fluorescence from each image. The observed timing of nucleic acid release for each short (and plasmid gene) DNA sequence follows the expected order of binding strength SS > SN > SX (TSS > TSN > TSX). The bidentate thiol exhibits nearly twice the half-life for DNA release ($t_{1/2} \sim 16$ h) when compared to the monodentate thiol ($t_{1/2} \sim 8$ h), and the mixed bidentate thiol and amine shows an intermediate release ($t_{1/2} \sim 12$ h) (Table 1). Overall displaying faster rates of DNA release for the monodentate versus bidentate and, similarly, a faster release rate for mixed strength
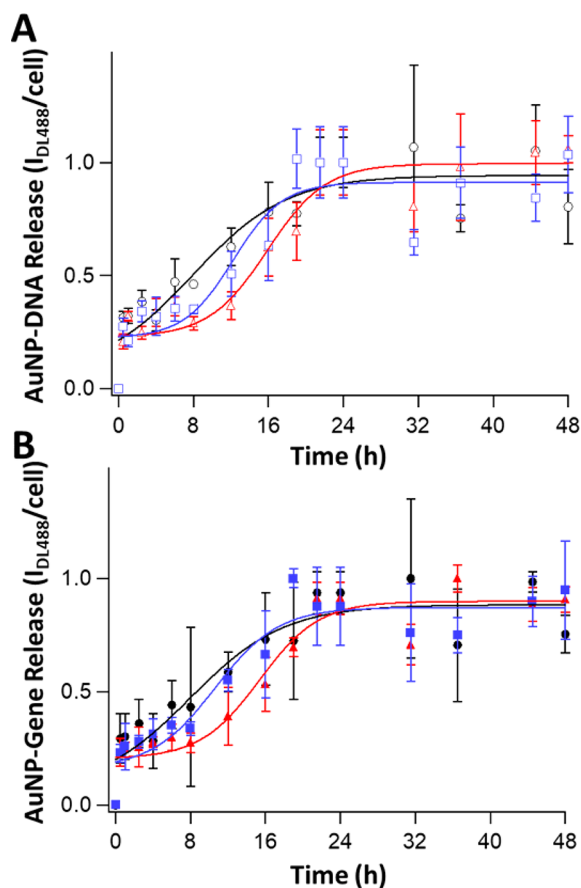
Figure 5. Kinetic data of SX (black circle), SS (red triangle), and SN (blue square) coupling strategies for AuNP attachment showing cellular cargo release, monitored by DL488 fluorescence intensity per cell, for short DNA (A, open symbols) and plasmid gene DNA (B, filled symbols), respectively. Trend lines reflect sigmoidal fits.

Table 1. Intracellular DNA Cargo Release Kinetics from 6 nm AuNP for Monodentate Thiol (AuNP-SX-DNA and AuNP-TSX-Gene), Bidentate Dual Thiol (AuNP-SS-DNA and AuNP-TSS-Gene), and Mixed Bidentate Thiol Plus Amine (AuNP-SN-DNA and AuNP-TSN-Gene) Attachment, for Short DNA Oligonucleotides and Linearized Plasmids, Respectively.

AuNP-Construct	$t_{1/2}$ (h)	DNA Release Rate ($\%\cdot h^{-1}$)
SX-DNA	7.9 ± 4.9	6.3 ± 0.2
SS-DNA	15.9 ± 1.5	3.2 ± 0.7
SN-DNA	12.2 ± 2.0	4.1 ± 0.5
TSX-Gene	8.0 ± 4.9	6.3 ± 0.2
TSS-Gene	15.4 ± 1.5	3.3 ± 0.7
TSN-Gene	10.6 ± 1.9	4.7 ± 0.5

coordinators (S and NH$_2$) *versus* the dual thiol is consistent with the amine having a bond dissociation energy from the (111) Au surface of 28.9 kJ/mol[51] compared to the thiol-Au bond having a dissociation energy of 253.6 kJ/mol.[52] The half-life ($t_{1/2}$) and DNA release rate for each coupling strategy is summarized in Table 1.

Impact of Coupling on tdTomato Expression. Functional expression of the gene requires delivery of the intact gene to the nuclear envelope, which may be time dependent due to endolysosomal processing. Expression of the tdTomato gene is signaled by whole cell fluorescence turn-on, as the RFP

is cytosolically overexpressed by the CMV promotor, engineered into the plasmid sequence. The onset of tdTomato fluorescence provides qualitative analysis of the influence of coupling strategies and the observed delay in endosomal release on gene expression yields.

In Figure 6A, fluorescence microscopy images reveal the influence on the timing and extent of gene expression of the TSX, TSS, and TSN linearized plasmids bound to the AuNP surface, as compared to lipofectamine-alone delivered TSS linearized plasmid in the absence of the AuNP. The progression of fluorescent protein expression can be seen for the various AuNP delivery constructs from 24 to 72 h. From the microscope images, TSX is observed to maintain a somewhat constant expression level after 36 h, whereas both TSS and TSN exhibit a steady increase in brightness from increased tdTomato expression in time (Figure 6A). The delay in expression is longest for the TSS sequence, consistent with the delayed intracellular release observed in Figure 5, and with the expected binding strength of the bidentate thiol linkage chemistry. Visual analysis of the number of expressing cells reveals the TSX to have maximal expression within 24 h post transfection, corresponding to 28% gene expression per cell, and after 36 h, expansion of the cell population exceeds the number of new cells expressing the tdTomato RFP (Supporting Information Figure SF9). However, comparing these results to the quantitative analysis of the gene expression intensity per cell over time, the observed fluorescence intensity per cell continues to increase in time, indicating that while no new cell transfection events are occurring, the tdTomato RFP continues to be expressed throughout the experiment (Figure 6B). Figure 6B also shows that TSN and TSS experiences maximal relative expression by 36 h, corresponding to 10% and 11% of cells expressing the RFP, respectively (Supporting Information Figure SF10), with degrees of variation over time being due to sampling statistics within a biological system. The linearized plasmid exhibits approximately uniform relative gene expression over the 72 h experimental time frame, with approximately 13% of cells expressing RFP over the 72 h (Figure 6B and Supporting Information Figure SF9). The apparent decreases in relative cellular expression levels in time seen in Supporting Information Figure SF10 can likely be attributed to the observation that the proliferation of the cells eventually exceeds the transfection rate.

■ CONCLUSION

Utilizing differential surface appendage strategies for coupling nucleic acid cargo to a AuNP delivery vehicle was shown to provide control over the timing of activation of nucleic acid sequences designed to knock-in (linear plasmid) protein expression *in vitro*. Through the use of SET-BOT probes, the delivery agent uptake, endosomal encapsulation and processing, and subsequent protein expression was visualized and quantified. It was found that a monodentate thiol ((T)SX) linkage to the AuNP surface provides the fastest intracellular release, followed by the mixed bidentate thiol plus amine ((T)SN) attachment, and finally the bidentate dual thiol ((T)SS) attachment. The observed order is consistent with the thermodynamics of a sulfur to gold *versus* sulfur to amine bond and predictions from inorganic chemistry and earlier self-assembled monolayer studies that show enhanced stabilization arises from back bonding with the gold d-orbital to sulfur empty p-orbital, which is more favorable in comparison to the σ-donor interaction of the nonbonding electrons on the amine,
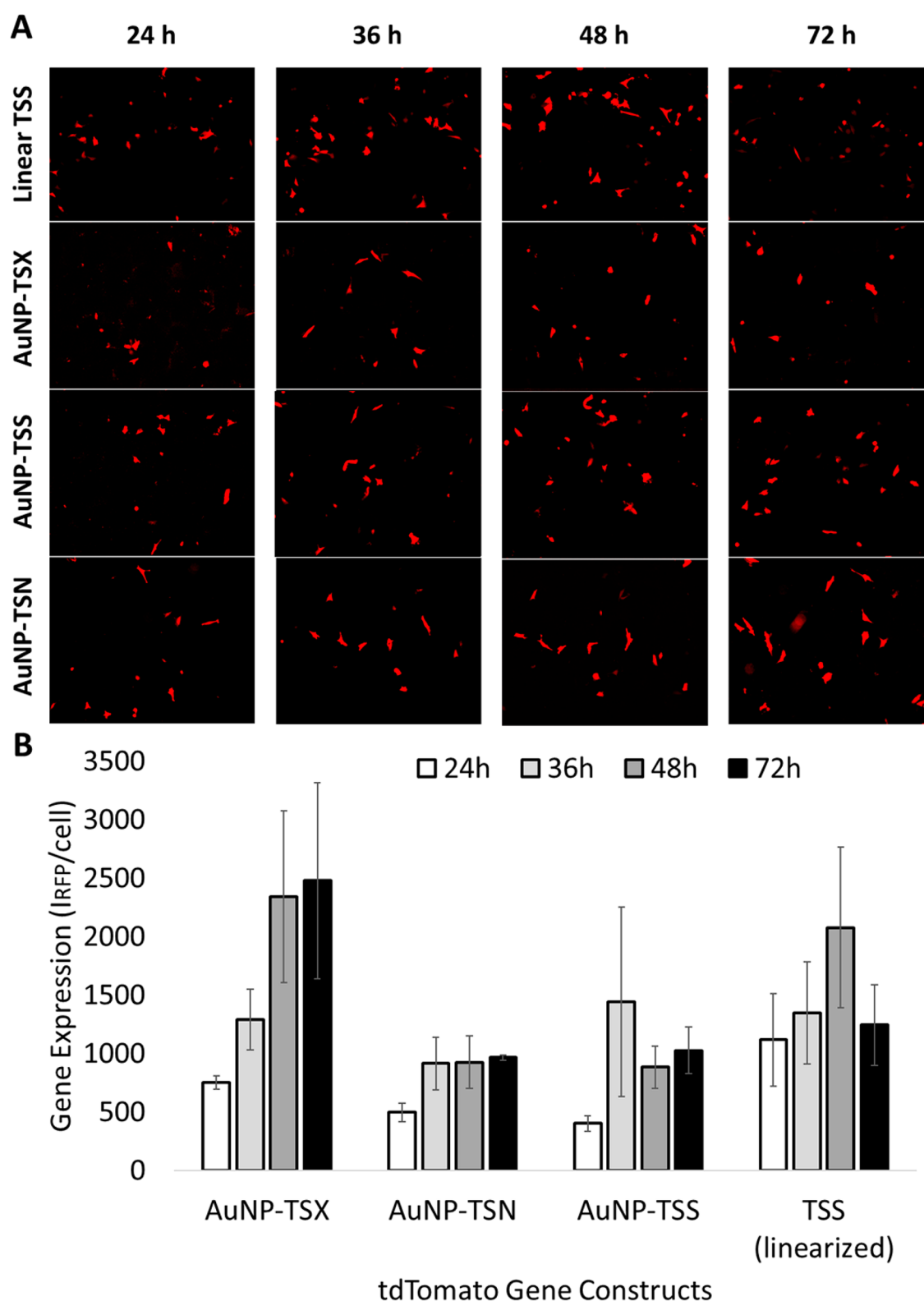
Figure 6. (A) Live cell fluorescent microscopy images of gene expression of the tdTomato red fluorescent protein from 24 to 72 h post transfection, for the linearized-plasmid with ligated dithiol-protected BOT sequence (Linear TSS), as well as the BOT-gene delivered by the AuNP *via* monodentate thiol (AuNP-TSX), bidentate thiol (AuNP-TSS), or mixed bidentate thiol plus amine (AuNP-TSN) DNA linkage. Scale bar is 100 μm. (B) Quantification of cellular gene expression of the tdTomato RFP from 24 to 72 h post transfection for the AuNP-TSX, AuNP-TSS, and AuNP-TSN attachment strategies, along with the linearized plasmid functionalized with dithiol protected short DNA modifications, as a control.

when coupling to the gold surface. Likewise, enhanced stabilization is attributed to the bidentate chelation.

Quantification of the expression of the various coupling strategies compared to the linearized plasmid without the AuNP further emphasizes the effect of delayed release on the

expression rate for the AuNP-TSX, -TSS, and -TSN, where for AuNP-TSX the level of expression is significantly greater at 24 h than observed at 36 h, in contrast to the bidentate thiols and mixed bidentate thiol plus amine. The similarity in total expression suggests no endosomal damage to the linearized plasmid occurs in the endosome, perhaps reflecting a pH damping effect reported by our group previously.[12] Interestingly, in the A375 cells the uptake and release dynamics for short DNA *versus* the plasmid is nearly identical. The observation is in contrast to earlier studies where the timing of release was observed to vary between the DNA lengths presumed to be due to the added molecular weight and charge density of the large plasmid compared to the short DNA oligonucleotide.[2] It is believed the differences are due to a reduction of the DNA loading levels in these studies, allowing access of small molecules in the endosome to cleave the nucleic acid sequence from the gold surface more effectively. Although not shown in this manuscript, the same coupling strategy could be employed to control timing between knock-in and knock-out of protein expression for cell biology studies. Competitive knock-in and knock-out was shown previously by our group to be effective for single thiol linkers.[7]

■ EXPERIMENTAL SECTION

Materials. Water-soluble, spherical 6.0 nm AuNP were synthesized by standard literature protocols for aqueous AuNP citrate nanoparticles.[6] Briefly, a sparged aqueous solution of tetrachloroauric acid hydrate (Strem Chemicals) was reduced in the presence of citric acid and tannic acid (Sigma) at 60 °C with rapid stirring at a ratio of 1:4:0.5 mL of each 1% m/v solution in 100 mL H_2O total volume. The prepared AuNPs were exchanged with bis(p-sulfantophenyl) phenylphosphine (bSPP) (Sigma) as the protecting group. Stoichiometric displacement of the coordinated BSPP passivation layer was accomplished by thiol place exchange reactions using 5′ thiol terminated DNA sequences, as described previously.[7] The synthetic DNA sequences were purchased from Midland Oligos and are listed in Supporting Information.

Preparation of AuNP-SX/SS/SN-DNA. AuNP-SX-DNA was prepared by complete thiol place exchange of the bSPP passivation layer using a 5′-C_6 thiol with or without a 3′-C_6 thiol or amine terminated short duplex DNA, to give the SX (monodentate thiol), SS (bidentate dual thiols), and SN (mixed bidentate thiol and amine) linkages. The DNA consisted of a synthetic 35 bp sequence with a 4 base overhang containing a 5′-C_6 thiol or amine and an internal DL488 dye label incorporated at the 10th bp and a complementary strand with 3′-C_6 thiol (SS) or amine (SN) modification, or unmodified 3′ (SX), with an internal DL700 dye label incorporated at the 30th bp. Dyes were incorporated through internal modification of the dT base. The exchange was carried out in a 20:1 mol ratio of DNA to AuNP, in the presence of reducing agent, tris(2-carboxyethyl)phosphine (Sigma), resulting in displacement of ∼20 passivating sites on the AuNP surface. The loading of the DNA was confirmed by gel electrophoresis (1% agarose) indicated a single red band that was more strongly retained than the AuNP-bSPP, consistent with formation of AuNP-DNA.

Preparation of AuNP-TSX/TSS/TSN-Plasmid Constructs. The AuNP-TSX/TSS/TSN-plasmid constructs were prepared by initial assembly of a linearized plasmid, appended to the SX/SS/SN linker sequences (with DL488 and DL700 internal labeling), to the AuNP surface by thiol place exchange,

in the presence of reducing agent, tris(2-carboxyethyl)-phosphine (Sigma). The dye labels for each sequence were located on the 30th bp from the terminal thiol modification via an internal labeling of the T base.

The linker modified plasmid was prepared using the commercially available tdTomato-C1 plasmid (Clontech) digested with PciI (New England Biolabs (NEB)) following the manufacturer's protocol. The plasmid contained a CMV promoter to ensure overexpression of the fluorescent protein within the cell following the translation of the delivered plasmid. The digested plasmid (single cut site) was analyzed on a 1% agarose gel to validate digestion. The synthetic SX/SS/SN-DNA linker strands (35/39 bp) contained a 4 base single stranded DNA overhang in order to be ligated to the linearized plasmid by standard T4 ligation methods (NEB) to create tdTomato plasmids with protected 5′-C_6 thiol modification with or without (TSX) a complementary 3′-C_6 protected thiol (TSS) or amine (TSN) modification to the phosphate backbone. The sequences are available in Supporting Information. The ligated plasmids, containing the chemically protected functional spacers, were precipitated by addition of ethanol and stored at 4 °C. Isolation of the linearized DNA was verified by UV−visible analysis of the 260 nm absorption for DNA.

The protected dithiol on the ligated BOT-plasmid was appended to the AuNP through reduction of the protecting group via TCEP (20 mM, 2 h, RT) incubation and subsequent formation of the AuNP-sulfur bond (AuNP-TSX-plasmid), dual AuNP-sulfur bonds (AuNP-TSS-plasmid), or AuNP-sulfur and AuNP-amine bonds (AuNP-TSN-plasmid), at a ratio of 1:1 plasmid to AuNP. Coupling of the plasmid to the AuNP surface was carried out by addition of the deprotected plasmid to a solution containing the AuNP and allowed to place exchange for 48 h. The assembled AuNP-TSX/TSS/TSN-plasmids were pelleted out of solution by ethanol precipitation followed by centrifugation at 3000 RPM to remove unbound plasmid.

SET-BOT Characterization. Size and shape analysis of the as-synthesized AuNPs was conducted using TEM images from a JEM-ARM200cF (JEOL USA) using 300 mesh carbon grids (Ted Pella), and particle diameters were measured in ImageJ software for manual measurement of the 100 particles. Preparation and analysis of 1% agarose gel electrophoresis of the as-synthesized AuNPs as compared to the AuNP-DNA and AuNP-plasmid constructs was performed at 25 °C, 80 V, and 500 mA to confirmed construct assembly, and showed <1% free AuNP present. Absorbance spectroscopy (Cary Bio-50) was performed to ascertain successful DNA loading on the particle surface by observation of the 260 nm DNA absorbance peak (ε_{260}: 4.1 × 10^5), as well as the 490 nm DL488 absorbance peak (ε_{488}: 7.0 × 10^4), and the 700 nm DL700 absorbance peak (ε_{700}: 1.4 × 10^5), in addition to the 525 nm absorbance peak of the AuNP plasmon (ε_{525}: 9.7 × 10^7). Photoluminescence emission spectroscopy (Varian Excite) was used to verify SET behavior of the DL488 and non-SET behavior of the DL700 fluorescent dye labels, by assessing peak intensity (ex./em. were 480/520 nm and 670/720 nm, respectively) before and after 0.1 M sodium cyanide incubation of 20 min. Dynamic light scattering was performed using a Möbius DLS (Wyatt) in DI water performed in triplicate with 10 scans of 10 s collection time, to determine average hydrodynamic diameter and size dispersity.

Transfection Agent. The AuNP transfection construct was prepared by encapsulating AuNP-SX-DNA, -SS-DNA, -SN-DNA, -TSX-plasmid, -TSS-plasmid, -TSN-plasmid into Lipofectamine2000 (Life Technologies). Lipofectamine2000 encapsulation of the AuNP constructs was carried out at a concentration of 3 pmol of AuNP, as determined by the AuNP absorption plasmon at 525 nm, to 10 μL of Lipofectamine2000. The loading level of constructs into the liposome was chosen to be consistent with concentrations utilized in the protocol for a standard plasmid transfection in Lipofectamine2000.[8] Dynamic Light Scattering (DLS) data (Wyatt Möbius) was obtained at 20% laser power and used to analyze the size of the transfection packages. The hydrodynamic radius is calculated by averaging 3 replicates each containing 10 measurements with an acquisition time of 10 s, with the complexes suspended in nanopure water.

Cell Transfection. A375 human melanoma cells, cultured at 37 °C with 5% CO_2 in Dulbecco's Modified Eagle's Medium (DMEM-7777) (Sigma) supplemented with addition of 10% fetal bovine serum (Sigma) were plated at 30,000/cm² in 0.33 cm² wells of a glass bottom 96-well plate or with 1.5 coverglass treated with poly(L-lysine) (MatTek Co.). Cellular transfection was carried out 24 h after plating. Media was exchanged after 48 h of transfection to remove any unreacted AuNP complex. Cell viability was verified using Trypan blue exclusion test of cell viability after 24 h, in addition to visual conformation on the microscope to assess the cell health. No significant evidence of chromosomal condensation or changes in cell morphology was observed following transfection, indicative of no cytotoxicity at the transfection agent concentrations employed in this study. Trypan blue assays confirmed cell viability was maintained at 90% following transfection for all experiments relative to control cells. Cell division was occurring over the time span of the experiment, with a doubling rate of 2% per hour resulting in confluence at 48 h. Due to confluence affecting cell growth behavior the experimental kinetics data was limited to 48 h measurements, and the gene expression studies were limited to 72 h. Experiments were conducted in triplicate.

Optical Microscopy. Confocal microscopy images were obtained on a Nikon Eclipse Ti Inverted Epifluorescence Microscope at 20× magnification. Samples were excited to collected emission of the DyLight700 (640 nm, 900 ms exposure), DyLight488 (488 nm, 500 ms exposure), and tdTomato (561 nm, 400 ms exposure). Images were collected by a Coolsnap-HQ10 high resolution CCD at 20× magnification. Measurements were taken over 48−72 h while live cells were incubated in a stage mounted live-cell chamber, kept in focus by a Nikon Perfect Focus system. Images were analyzed for total intensity and cell number by ImageJ software. Intracellular uptake and release kinetics were monitored by tracking DyLight700 and DyLight488 intensities, respectively, normalized to cell count.

Image Analysis. The kinetics of the images were analyzed with ImageJ software, using a standard rolling ball radius of 50 pixels to subtract the background to remove any cellular autofluorescence and the total intensity of each image was measured per time frame. The resulting intensity was corrected for cell count and plotted to sigmoidal model fit using Igor software, to compute the first order association kinetics of the release of the short duplex DNA and plasmid from the surface of the AuNP, plotted with standard deviation of the samples. Each experimental trial was imaged in three separate regions per well in a 96-well plate per time point, with $n = 3$ per sample. The plots were analyzed for differences using the Student's unpaired t test, to determine statistical differences in the samples. Protein expression was analyzed with ImageJ and RFP fluorescent intensity as well as the number of expressing cells was corrected to cell count per time fame. Colocalization of the DL700 and DL488 was analyzed using the JACoP[53] plugin for ImageJ to assess the van Steensel Cross Correlation Function (CCF) for DL700 versus DL488 fluorescence channels, with best Gaussian fit calculated per image per time point.

ASSOCIATED CONTENT

Ⓢ Supporting Information

The Supporting Information is available free of charge on the ACS Publications website at DOI: 10.1021/acs.bioconjchem.8b00575.

Synthetic DNA sequence information, TEM and size distribution of AuNPs, gel electrophoresis, absorption spectroscopy for each construct before and after cyanide etching, media stability data, the control live cell microscopy and digitally magnified individual cell images, SET-BOT cellular uptake and colocalization data, and tdTomato expression data presented as percentages (PDF)

AUTHOR INFORMATION

Corresponding Author

*E-mail: strouse@chem.fsu.edu.

ORCID

Kate J. F. Carnevale: 0000-0001-6898-0381
Geoffrey F. Strouse: 0000-0003-0841-282X

Author Contributions

The manuscript was written through contributions of all authors. All authors have given approval to the final version of the manuscript.

Notes

The authors declare no competing financial interest.

ACKNOWLEDGMENTS

REFERENCES

(1) Dean, K. M., and Palmer, A. E. (2014) Advances in fluorescence labeling strategies for dynamic cellular imaging. *Nat. Chem. Biol. 10*, 512−523.

(2) Muroski, M. E., Carnevale, K. J. F., Riskowski, R. A., and Strouse, G. F. (2015) Plasmid transfection in mammalian cells spatiotemporally tracked by a gold nanoparticle. *ACS Nano 9*, 124−133.

(3) Seferos, D. S., Giljohann, D. A., Hill, H. D., Prigodich, A. E., and Mirkin, C. A. (2007) Nano-flares: probes for transfection and mRNA detection in living cells. *J. Am. Chem. Soc. 129*, 15477−15479.

(4) Breshike, C. J., Riskowski, R. A., and Strouse, G. F. (2013) Leaving Forster Resonance Energy Transfer Behind: Nanometal Surface Energy Transfer Predicts the Size-Enhanced Energy Coupling between a Metal Nanoparticle and an Emitting Dipole. *J. Phys. Chem. C 117*, 23942−23949.

(5) Armstrong, R. E., Riskowski, R. A., and Strouse, G. F. (2015) Nanometal Surface Energy Transfer Optical Ruler for Measuring a Human Telomere Structure. *Photochem. Photobiol. 91*, 732−738.

(6) Armstrong, R. E., and Strouse, G. F. (2014) Rationally Manipulating Aptamer Binding Affinities in a Stem-Loop Molecular Beacon. *Bioconjugate Chem. 25*, 1769−1776.

(7) Muroski, M. E., Kogot, J. M., and Strouse, G. F. (2012) Bimodal Gold Nanoparticle Therapeutics for Manipulating Exogenous and Endogenous Protein Levels in Mammalian Cells. *J. Am. Chem. Soc. 134*, 19722−19730.

(8) Cheng, Y., Morshed, R. A., Auffinger, B., Tobias, A. L., and Lesniak, M. S. (2014) Multifunctional nanoparticles for brain tumor imaging and therapy. *Adv. Drug Delivery Rev. 66*, 42−57.

(9) Medarova, Z., Kumar, M., Ng, S. W., and Moore, A. (2009) Development and application of a dual-purpose nanoparticle platform for delivery and imaging of siRNA in tumors. *Methods Mol. Biol. 555*, 1−13.

(10) Cheon, J., and Lee, J. H. (2008) Synergistically integrated nanoparticles as multimodal probes for nanobiotechnology. *Acc. Chem. Res. 41*, 1630−1640.

(11) Muroski, M. E., Morgan, T. J. T. J., Levenson, C. W., and Strouse, G. F. (2014) A Gold Nanoparticle Pentapeptide: Gene Fusion To Induce Therapeutic Gene Expression in Mesenchymal Stem Cells. *J. Am. Chem. Soc. 136*, 14763−14771.

(12) Carnevale, K. J. F., Riskowski, R. A., and Strouse, G. F. (2018) A Gold Nanoparticle Bio-Optical Transponder to Dynamically Monitor Intracellular pH. *ACS Nano 12*, 5956−5968.

(13) Muroski, M. E., Carnevale, K. J. F., Riskowski, R. A., and Strouse, G. F. (2015) Plasmid transfection in Mammalian cells spatiotemporally tracked by a gold nanoparticle. *ACS Nano 9*, 124−133.

(14) Barnaby, S. N., Lee, A., and Mirkin, C. A. (2014) Probing the inherent stability of siRNA immobilized on nanoparticle constructs. *Proc. Natl. Acad. Sci. U. S. A. 111*, 9739−9744.

(15) de Puig, H., Cifuentes Rius, A., Flemister, D., Baxamusa, S. H., Hamad-Schifferli, K., and Antopolsky, M. (2013) Selective Light-Triggered Release of DNA from Gold Nanorods Switches Blood Clotting On and Off. *PLoS One 8*, e68511.

(16) Karimi, M., Ghasemi, A., Sahandi Zangabad, P., Rahighi, R., Moosavi Basri, S. M., Mirshekari, H., Amiri, M., Shafaei Pishabad, Z., Aslani, A., Bozorgomid, M., et al. (2016)et al Smart micro/nanoparticles in stimulus-responsive drug/gene delivery systems. *Chem. Soc. Rev. 45*, 1457−1501.

(17) Hong, R., Han, G., Fernández, J. M., Kim, B., Forbes, N. S., and Rotello, V. M. (2006) Glutathione-Mediated Delivery and Release Using Monolayer Protected Nanoparticle Carriers. *J. Am. Chem. Soc. 128*, 1078−1079.

(18) Li, D., Li, G., Guo, W., Li, P., Wang, E., and Wang, J. (2008) Glutathione-mediated release of functional plasmid DNA from positively charged quantum dots. *Biomaterials 29*, 2776−2782.

(19) Zhu, Z. J., Tang, R., Yeh, Y. C., Miranda, O. R., Rotello, V. M., and Vachet, R. W. (2012) Determination of the Intracellular Stability of Gold Nanoparticle Monolayers Using Mass Spectrometry. *Anal. Chem. 84*, 4321−4326.

(20) Nuzzo, R. G., Fusco, F. A., and Allara, D. L. (1987) Spontaneously Organized Molecular Assemblies. 3. Preparation and Properties of Solution Adsorbed Monolayers of Organic Disulfides on Gold Surfaces. *J. Am. Chem. Soc. 109*, 2358−2368.

(21) Allara, D. L., and Nuzzo, R. G. (1985) Spontaneously Organized Molecular Assemblies. 1. Formation, Dynamics, and Physical Properties of n-Alkanoic Acids Adsorbed from Solution on an Oxidized Aluminum Surface. *Langmuir 1*, 45−52.

(22) Sigal, G. B., Bamdad, C., Barberis, A., Strominger, J., and Whitesides, G. M. (1996) A Self-Assembled Monolayer for the Binding and Study of Histidine-Tagged Proteins by Surface Plasmon Resonance. *Anal. Chem. 68*, 490−497.

(23) Mrksich, M., and Whitesides, G. M. (1996) Using Self-Assembled Monolayers to Understand the Interactions of Man-made

Surfaces with Proteins and Cells. *Annu. Rev. Biophys. Biomol. Struct. 25*, 55−78.

(24) Östblom, M., Liedberg, B., Demers, L. M., and Mirkin, C. A. (2005) On the structure and desorption dynamics of DNA bases adsorbed on gold: A temperature-programmed study. *J. Phys. Chem. B 109*, 15150−15160.

(25) Li, Z., Jin, R., Mirkin, C. A., and Letsinger, R. L. (2002) Multiple thiol-anchor capped DNA-gold nanoparticle conjugates. *Nucleic Acids Res. 30*, 1558−62.

(26) Li, Z. (2002) Multiple thiol-anchor capped DNA-gold nanoparticle conjugates. *Nucleic Acids Res. 30*, 1558−1562.

(27) Li, F., Zhang, H., Dever, B., Li, X.-F., and Le, X. C. (2013) Thermal Stability of DNA Functionalized Gold Nanoparticles. *Bioconjugate Chem. 24*, 1790−1797.

(28) Kapur, A., Aldeek, F., Ji, X., Safi, M., Wang, W., Del Cid, A., Steinbock, O., and Mattoussi, H. (2017) Self-Assembled Gold Nanoparticle−Fluorescent Protein Conjugates as Platforms for Sensing Thiolate Compounds *via* Modulation of Energy Transfer Quenching. *Bioconjugate Chem. 28*, 678−687.

(29) Yeh, Y.-C., Creran, B., and Rotello, V. M. (2012) Gold nanoparticles: preparation, properties, and applications in bionano-technology. *Nanoscale 4*, 1871−1880.

(30) Han, G., Ghosh, P., and Rotello, V. M. (2007) Functionalized gold nanoparticles for drug delivery. *Nanomedicine (London, U. K.) 2*, 113−123.

(31) Li, F., Zhang, H., Dever, B., Li, X.-F., and Le, X. C. (2013) Thermal Stability of DNA Functionalized Gold Nanoparticles. *Bioconjugate Chem. 24*, 1790−1797.

(32) Kogot, J. M., England, H. J., Strouse, G. F., and Logan, T. M. (2008) Single Peptide Assembly onto a 1. 5 nm Au Surface *via* a Histidine. *J. Am. Chem. Soc. 130*, 16156−16157.

(33) Mei, B. C., Oh, E., Susumu, K., Farrell, D., Mountziaris, T. J., and Mattoussi, H. (2009) Effects of ligand coordination number and surface curvature on the stability of gold nanoparticles in aqueous solutions. *Langmuir 25*, 10604−10611.

(34) Susumu, K., Oh, E., Delehanty, J. B., Blanco-Canosa, J. B., Johnson, B. J., Jain, V., Hervey, W. J., Algar, W. R., Boeneman, K., Dawson, P. E., and Medintz, I. L. (2011) Multifunctional compact zwitterionic ligands for preparing robust biocompatible semi-conductor quantum dots and gold nanoparticles. *J. Am. Chem. Soc. 133*, 9480−9496.

(35) Liu, C., Leng, W., and Vikesland, P. J. (2018) Controlled Evaluation of the Impacts of Surface Coatings on Silver Nanoparticle Dissolution Rates. *Environ. Sci. Technol. 52*, 2726−2734.

(36) Hinterwirth, H., Kappel, S., Waitz, T., Prohaska, T., Lindner, W., and Lämmerhofer, M. (2013) Quantifying Thiol Ligand Density of Self-Assembled Monolayers on Gold Nanoparticles by Inductively Coupled Plasma−Mass Spectrometry. *ACS Nano 7*, 1129−1136.

(37) Hayat, M. A. (1989) *Colloidal gold : principles, methods, and applications*, Academic Press, New York.

(38) Tang, D.-C., Jennelle, R. S., Shi, Z., Garver, R. I., Carbone, D. P., Loya, F., Chang, C.-H., and Curiel, D. T. (1997) Overexpression of Adenovirus-Encoded Transgenes from the Cytomegalovirus Immediate Early Promoter in Irradiated Tumor Cells. *Hum. Gene Ther. 8*, 2117−2124.

(39) Hill, H. D., Millstone, J. E., Banholzer, M. J., and Mirkin, C. A. (2009) The role radius of curvature plays in thiolated oligonucleotide loading on gold nanoparticles. *ACS Nano 3*, 418−424.

(40) Hurst, S. J., Lytton-Jean, A. K. L., and Mirkin, C. A. (2006) Maximizing DNA Loading on a Range of Gold Nanoparticle Sizes. *Anal. Chem. 78*, 8313−8318.

(41) Maclaurin, R. C. (1893) The dissolution of gold in a solution of potassium cyanide. *J. Chem. Soc., Trans. 63*, 724−738.

(42) Yun, C. S., Javier, A., Jennings, T., Fisher, M., Hira, S., Peterson, S., Hopkins, B., Reich, N. O., and Strouse, G. F. (2005) Nanometal surface energy transfer in optical rulers, breaking the FRET barrier. *J. Am. Chem. Soc. 127*, 3115−3119.

(43) Breshike, C. J., Riskowski, R. A., and Strouse, G. F. (2013) Leaving FRET Behind, Size-Enhanced Energy Coupling Between a

Metal Nanoparticle and an Emitting Dipole. *J. Phys. Chem. C 117*, 23942−23949.

(44) Ghosh, P., Han, G., De, M., Kim, C. K., and Rotello, V. M. (2008) Gold nanoparticles in delivery applications. *Adv. Drug Delivery Rev. 60*, 1307−1315.

(45) Delehanty, J. B., Bradburne, C. E., Boeneman, K., Susumu, K., Farrell, D., Mei, B. C., Blanco-Canosa, J. B., Dawson, G., Dawson, P. E., Mattoussi, H., and Medintz, I. L. (2010) Delivering quantum dot-peptide bioconjugates to the cellular cytosol: Escaping from the endolysosomal system. *Integr. Biol. 2*, 265−277.

(46) Sangtani, A., Petryayeva, E., Wu, M., Susumu, K., Oh, E., Huston, A. L., Lasarte-Aragones, G., Medintz, I. L., Algar, W. R., and Delehanty, J. B. (2018) Intracellularly Actuated Quantum Dot−Peptide−Doxorubicin Nanobioconjugates for Controlled Drug Delivery *via* the Endocytic Pathway. *Bioconjugate Chem. 29*, 136−148.

(47) van Steensel, B., Brink, M., van der Meulen, K., van Binnendijk, E. P., Wansink, D. G., de Jong, L., de Kloet, E. R., and van Driel, R. (1995) Localization of the glucocorticoid receptor in discrete clusters in the cell nucleus. *J. Cell Sci. 108* (9), 3003−11.

(48) Manders, E. M. M., Verbeek, F. J., and Aten, J. A. (1993) Measurement of co-localization of objects in dual-colour confocal images. *J. Microsc. 169*, 375−382.

(49) Bolte, S., and Cordelieres, F. P. (2006) A guided tour into subcellular colocalization analysis in light microscopy. *J. Microsc. 224*, 213−232.

(50) Schindelin, J., Arganda-Carreras, I., Frise, E., Kaynig, V., Longair, M., Pietzsch, T., Preibisch, S., Rueden, C., Saalfeld, S., Schmid, B., Tinevez, J.-Y., White, D. J., Hartenstein, V., Eliceiri, K., Tomancak, P., and Cardona, A. (2012) Fiji: an open-source platform for biological-image analysis. *Nat. Methods 9*, 676−682.

(51) Hoft, R. C., Ford, M. J., McDonagh, A. M., and Cortie, M. B. (2007) Adsorption of Amine Compounds on the Au(111) Surface: A Density Functional Study. *J. Phys. Chem. C 111*, 13886−13891.

(52) Luo, Y.-R., and Luo, Y.-R. (2007) *Comprehensive handbook of chemical bond energies*, CRC Press.

(53) Cordelières, F. P., and Bolte, S. (2008) JACoP v2.0 : improving the user experience with co-localization studies, pp 174−181, In Proceedings of the ImageJ User and Development Conference.